WALAILAK JOURNAL
http://wjst.wu.ac.th Engineering and Physical Sciences

Flow and Heat Transfer in MHD Dusty Nanofluid Past a Stretching/ Shrinking Surface with Non-Uniform Heat Source/Sink

Naramgari SANDEEP[1], Chalavadi SULOCHANA[1] and Banglore Rushi KUMAR[2,*]

[1]*Department of Mathematics, Gulbarga University, Gulbarga 585106, India*
[2]*Fluid Dynamics Division, VIT University, Vellore 632014, India*

([*]Corresponding author's e-mail: rushikumar@vit.ac.in)

Received: 26 April 2015, Revised: 2 October 2015, Accepted: 18 November 2015

Abstract

The present study concerns the momentum and heat transfer characteristics of magnetohydrodynamic (MHD) dusty nanofluid flow over a permeable stretching/shrinking surface in the presence of a volume fraction of dust and nanoparticles with non-uniform heat source/sink. We consider 2 types of nanofluids, namely, TiO_2-water and Al_2O_3-water, embedded with conducting dust particles. The governing partial differential equations of the flow and heat transfer are transformed to nonlinear ordinary differential equations by using a similarity transformation and are solved numerically using a Runge-Kutta based shooting technique. The effects of non-dimensional governing parameters on velocity and temperature profiles for both fluid and dust phases are discussed for both stretching and shrinking cases and presented through graphs. Also, skin friction coefficient and heat transfer rate is discussed and presented in tabular form for the 2 dusty nanofluids separately.

Keywords: MHD, dusty nanofluid, stretching/shrinking surface, volume fraction, non-uniform heat source/sink

Nomenclature:

u, v	velocity components of fluid phase in x and y directions (m)
u_p, v_p	velocity components of dust phase in x and y directions (m)
x	distance along the surface (m)
y	distance normal to the surface (m)
c_p	specific heat capacity at constant pressure (J/KgK)
f, F	dimensionless velocities
T	temperature of the fluid phase (K)
T_p	temperature of the particle phase (K)
m	mass of the particle phase (g)
q'''	non-uniform heat source/sink (W/m^3)
k_f	thermal conductivity of the base fluid (W/mK)

Greek Symbols

η	similarity variable
β_T	volumetric thermal expansion (K^{-1})
θ	dimensionless temperature (K)
ρ_f	fluid density (Kg/m^3)
ν	kinematic viscosity (m^2/s)
μ_f	dynamic viscosity (Ns/m^2)
ϕ	nano particle volume fraction (nm)
ϕ_d	dust particle volume fraction (μm or mm)

$(\rho c_p)_f$ heat capacity of the fluid (Kg/m^3K)

$(\rho c_p)_s$ effective heat capacity of the nano particle medium (Kg/m^3K)

Non-dimensional parameters

A^*, B^* non-uniform heat generation/absorption coefficients
C_f skin friction coefficient in x-direction
Nu_x local Nusselt number
Re_x local Reynolds number
Pr Prandtl number
K number density of dust particles
c positive constant
α mass concentration of dust particles
β fluid particle interaction parameter
B_0 magnetic induction parameter
τ_v relaxation time of the dust particles
S suction/injection parameter
M magnetic field parameter
λ stretching/shrinking parameter

Subscripts

f fluid
s solid
∞ condition at the free stream
nf nanofluid

Introduction

Momentum and heat transfer characteristics of magnetohydrodynamic MHD flows over a stretching/shrinking surface have vast applications in engineering and applied sciences. Over the past few decades many researchers have investigated the momentum and heat transfer characteristics of either dusty or nanofluids through different channels. Nowadays, low thermal conductivity, in convectional fluids like water, ethylene glycol, oil etc., raises a variety of problems in engineering electronic devices. To overcome these drawbacks and enhance the thermal conductivity in convectional fluids, over the past few decades, many researchers have concentrated on the mixing of nano- or micrometer sized particles in the base fluids. In the present study, we take the initiative to analyze the momentum and heat transfer characteristics of a dusty nanofluid (a nanofluid embedded with dust particles) over a stretching/shrinking surface by considering a volume fraction of dust particles (in μm) and a volume fraction of nanoparticles (in *nm*). This has potential applications in the fields of industrial engineering, aerospace, aeronautics, medicine, science, and technology, such as in metal and polymer extrusion, chemical processing equipment, exchangers, etc.

The laminar flow of dusty gases was first discussed by Saffman [1]. The behavior of dusty gases in different environments was first analyzed by Marble [2]. Chakrabarti and Gupta [3] studied MHD flow and heat transfer characteristics over a stretching surface. Choi [4] was the first person to introduce the concept of a nanofluid. He immersed nanometer sized particles into a base fluid and observed the increase in heat transfer rate in a nanoparticle mixed base fluid. Singh and Singh [5] studied dusty viscoelastic MHD flow through inclined parallel plates by considering a porous medium. Chen [6] discussed mixed convection flow of a nanofluid adjacent to a vertical and continuous stretching sheet. Dalal *et al*. [7] discussed unsteady flow of a dusty fluid over a rectangular channel. Attia [8] analyzed MHD dusty fluid flow at different physical properties. Buongiorno [9] studied convective heat transfer phenomenon in nanofluids. A book written by Das *et al*. [10] gave a clear description of the applications of nanofluids in science and technology.

Wang and Mujumdar [11] investigated the heat transfer characteristics of nanofluids by immersing different types of nanoparticles into base fluids. Subhas Abel *et al*. [12] studied MHD flow of a viscoelastic fluid through a stretching surface with viscous and ohmic dissipations. Ishak *et al*. [13] analyzed the heat transfer characteristics of a nanofluid over a permeable stretching surface. Prasad *et al*. [14] discussed the effects of different fluid properties of MHD flowing past a nonlinear stretching sheet.

Saidu and Waziri [15] analyzed MHD flow of dusty fluid by considering a volume fraction of dust particles. Makinde and Aziz [16] discussed boundary layer flow of a nanofluid through a stretching sheet by considering convective boundary conditions. Hamad and Pop [17] studied MHD free convection flow of a nanofluid over a flat plate in a rotating frame with heat source. Stagnation point flow of a nanofluid over a heated stretching sheet, considering suction/injection effects, was analyzed by Hamad and Ferdows [18]. Gireesha *et al*. [19] discussed MHD flow and heat transfer characteristics of a dusty fluid past a stretching sheet.

Remeli *et al*. [20] analyzed Marangoni-driven boundary layer flow of a nanofluid by considering suction/injection effects. Zaimi *et al.* [21] studied nanofluid flow over a permeable stretching/shrinking sheet by considering a 2 phase model. Ferdows *et al*. [22] discussed the heat transfer characteristics of boundary layer nanofluid flow with viscous dissipation over an unsteady stretching sheet. The unsteady stagnation point flow of a nanofluid over a stretching surface was illustrated by Malyand *et al.* [23]. Rohni *et al*. [24] analyzed the momentum and heat transfer characteristics of a nanofluid past an exponentially shrinking vertical sheet by considering suction effects. Subhashini *et al.* [25] presented dual solutions for mixed convection flow of a nanofluid near the stagnation point region over an exponentially stretching/shrinking sheet. Krishnamurthy *et al.* [26] discussed the MHD and heat transfer of nanofluid with fluid particle suspension. Further, Krishnamurthy *et al.* [27] studied the effects of chemical reaction on MHD boundary layer flow and melting heat transfer of non-Newtonian nanofluid. Stagnation-point flow and convective heat transfer of a Williamson nanofluid past a stretching/shrinking sheet was discussed by Gorla and Gireesha [28]. Recently, the researchers [29-31] analyzed the heat and mass transfer characteristics of magnetic flows through different channels. Abbas *et al.* [32] discussed the influence of thermal radiation on MHD flow over a stretching cylinder in porous medium. Javid and Mustafa [33] analyzed the stagnation flow of an unsteady Wang problem in the presence of suction. Further, Mustafa *et al.* [34] studied the MHD mixed convection stagnation point flow of a nanofluid over a vertical plate with viscous dissipation.

All the above studies focused on either dusty or nanofluid flows through different channels. To the best of our knowledge, the present study is a new initiative, and no studies have been reported on the momentum and heat transfer characteristics of MHD flow of a dusty nanofluid over a permeable stretching/shrinking surface in the presence of a volume fraction of dust and nanoparticles with non-uniform heat source/sink. We consider TiO_2-water and Al_2O_3-water nanofluids immersed with dust particles. The governing partial differential equations of the flow and heat transfer are transformed into nonlinear ordinary differential equations and solved numerically. The effects of non-dimensional governing parameters on velocity and temperature profiles for both fluid and dust phases are discussed and presented graphically. Also, skin friction coefficient and Nusselt number are discussed and presented in tabular form for 2 dusty nanofluids.

Materials and methods

Flow analysis

Consider a steady, 2 dimensional, laminar, incompressible, and electrically conducting boundary layer flow of a dusty nanofluid over a permeable stretching/shrinking sheet. The sheet is along the plane $y = 0$, with the flow being confined to $y > 0$. The flow is generated by 2 equal and opposite forces acting along the x-axis, and the y-axis is normal to it. The flow field is exposed to the influence of an external magnetic field strength B_0 along the x-axis as shown in **Figure 1**. Induced magnetic field is neglected in this study. The dust particles are assumed to be uniform in size. Spherical shaped nano and dust particles are considered. The number density of the dust particles, along with the volume fraction of the dust and nanoparticles, is taken into account.

The boundary layer equations that govern the present flow, as per the above assumptions, are [15,19];

$$\frac{\partial u}{\partial x}+\frac{\partial v}{\partial y}=0, \tag{1}$$

$$\rho_{nf}(1-\phi_d)\left(u\frac{\partial u}{\partial x}+v\frac{\partial u}{\partial y}\right)=(1-\phi_d)\mu_{nf}\frac{\partial^2 u}{\partial y^2}+KN(u_p-u)-\sigma B_0{}^2u, \tag{2}$$

$$u_p\frac{\partial u_p}{\partial x}+v_p\frac{\partial u_p}{\partial y}=\frac{K}{m}(u-u_p), \tag{3}$$

$$\frac{\partial u_p}{\partial x}+\frac{\partial v_p}{\partial y}=0, \tag{4}$$

with the boundary conditions;

$$u=\lambda U_w(x), v=v_w \text{ at } y=0,$$
$$u\to 0, u_p\to 0, v_p\to v \text{ as } y\to\infty, \tag{5}$$

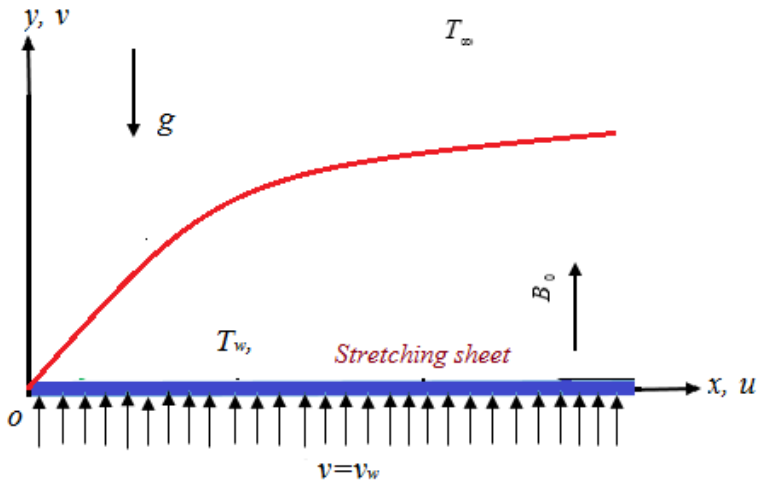

Figure 1 Physical model of the problem.

where (u,v) and (u_p,v_p) are the velocity components of the nanofluid and dust phases in the x and y directions respectively, ϕ_d is the volume fraction of the dust particles (i.e., the volume occupied by the dust particles per unit volume of mixture), μ_{nf} is the dynamic viscosity of the nanofluid, K is the Stokes resistance, m is the mass of the dust particle, N is the number density of the dust particles, ρ_{nf} is the density of the nanofluid, σ, B_0 are the electrical conductivity and external magnetic field, respectively, and λ is the stretching/shrinking parameter, with $\lambda>0$ for a stretching surface and $\lambda<0$ for a shrinking surface. It is assumed that the surface is stretched or is shrunk with the velocity

$U_w(x) = cx, c > 0$ is constant, and v_w is the suction or injection velocity, with $v_w < 0$ for suction and $v_w > 0$ for injection. The nanofluid constants are given by;

$$(\rho c_p)_{nf} = (1-\phi)(\rho c_p)_f + \phi(\rho c_p)_s,$$
$$\frac{k_{nf}}{k_f} = \frac{(k_s + 2k_f) - 2\phi(k_f - k_s)}{(k_s + 2k_f) + \phi(k_f - k_s)}, \quad \mu_{nf} = \frac{\mu_f}{(1-\phi)^{2.5}}, \quad \rho_{nf} = (1-\phi)\rho_f + \phi\rho_s, \tag{6}$$

where ϕ is the volume fraction of the nanoparticles. The subscripts f and s refer to fluid and solid properties, respectively.

For a similarity solution, we introduce the following similarity transformation;

$$u = cxf'(\eta), \; v = -\nu_f^{1/2} c^{1/2} f(\eta), \; \eta = \nu_f^{-1/2} c^{1/2} y,$$
$$u_p = cxF'(\eta), \; v_p = -\nu_f^{1/2} c^{1/2} F(\eta), \tag{7}$$

where Eq. (7) identically satisfies Eq. (1) and Eq. (4). Now, using Eqs. (5) - (7) and Eq. (15), Eq. (2) and Eq. (3) reduce to;

$$\frac{1-\phi_d}{(1-\phi)^{2.5}} f''' - (1-\phi_d)\left(1 - \phi + \phi\left(\frac{\rho_s}{\rho_f}\right)\right)(f'^2 - ff'') + \alpha\beta(F' - f') - Mf' = 0, \tag{8}$$

$$F'^2 - FF'' + \beta(F' - f') = 0, \tag{9}$$

with the transformed boundary conditions;

$$f'(\eta) = \lambda, \; f(\eta) = S \text{ at } \eta = 0,$$
$$f'(\eta) = 0, \; F'(\eta) = 0, \; F(\eta) = f(\eta) \text{ as } \eta \to \infty, \tag{10}$$

where $\alpha = Nm/\rho_f$ is the mass concentration of the dust particles, $\beta = K/cm$ is the fluid particle interaction parameter for the velocity, $M = \sigma B_0^2 / c\rho_f$ is the magnetic field parameter, and $v_w = -\sqrt{c\nu}\, S$, where the constant parameter S corresponds to suction for $S > 0$ and injection for $S < 0$.

Heat transfer analysis

The governing boundary layer heat transport equations for dusty nanofluid are ;

$$(\rho c_p)_{nf}\left(u\frac{\partial T}{\partial x} + v\frac{\partial T}{\partial y}\right) = k_{nf}\frac{\partial^2 T}{\partial y^2} + \frac{N_1(c_p)_f}{\tau_T}(T_p - T) + \frac{N_1}{\tau_v}(u_p - u)^2 + q''', \tag{11}$$

$$N_1 c_m \left(u_p \frac{\partial T_p}{\partial x} + v_p \frac{\partial T_p}{\partial y} \right) = -\frac{N_1 (c_p)_f}{\tau_T} (T_p - T), \tag{12}$$

where T and T_p are the temperatures of the nanofluid and dust particles, respectively, k_{nf} is the effective thermal conductivity of the nanofluid, $(c_p)_f, c_m$ are the specific heat levels of the fluid and dust particles, respectively, $N_1 = Nm$ is the density of the particle phase, τ_T is the thermal equilibrium time, and τ_v is the relaxation time of the dust particle. The space and temperature dependent heat generation/absorption (non-uniform heat source/sink) q''' is defined as per Sandeep and Sulochana [30];

$$q''' = \left(\frac{k_f U_w(x)}{x \nu_f} \right) \left(A^* (T_w - T_\infty) f'(\eta) + B^* (T - T_\infty) \right), \tag{13}$$

where A^* and B^* are parameters of the space- and temperature-dependent internal heat generation/absorption. The positive and negative values of A^* and B^* represent the heat generation and absorption, respectively.

We consider temperature boundary conditions in order to solve Eqs. (11) - (13) as;

$$\begin{aligned} &T = T_w = T_\infty + A\left(x/l\right)^2 \quad \text{at } y = 0, \\ &T \to T_\infty, T_p \to T_\infty \quad \text{as } y \to \infty, \end{aligned} \tag{14}$$

where T_w, T_∞ are the temperatures near the wall and far away from the wall, respectively, and $l = \nu_f^{1/2} c^{-1/2} > 0$ is a characteristic length.

We now introduce the following non-dimensional variables to obtain the similarity solutions of Eqs. (11) - (13);

$$\theta(\eta) = \frac{T - T_\infty}{T_w - T_\infty}, \theta_p(\eta) = \frac{T_p - T_\infty}{T_w - T_\infty}, \tag{15}$$

where $T - T_\infty = A(x/l)^2 \theta(\eta), A > 0,$

Using Eqs. (6), (7), (14), and (15) in Eqs. (11) - (13), we obtain the ordinary differential equations;

$$\begin{aligned} &\frac{1}{\Pr} \frac{k_{nf}/k_f}{1-\phi+\phi\left((\rho c_p)_s/(\rho c_p)_f\right)} \theta'' - (2f'\theta - f\theta') + \frac{1}{1-\phi+\phi\left((\rho c_p)_s/(\rho c_p)_f\right)} \left[\alpha\beta_T(\theta_p - \theta) + Ec\alpha(F' - f')^2 \right] \\ &+ \frac{1}{\Pr} \frac{1}{1-\phi+\phi\left((\rho c_p)_s/(\rho c_p)_f\right)} \left[A^* f' + B^* \theta \right] = 0 \end{aligned} \tag{16}$$

$$2F'\theta_p - F\theta_p' + \gamma\beta_T(\theta_p - \theta) = 0 \tag{17}$$

with the transformed boundary conditions;

$$\theta(\eta) = 1 \text{ at } \eta = 0$$
$$\theta(\eta) = 0, \theta_p(\eta) = 0 \text{ as } \eta \to \infty \tag{18}$$

where $\Pr = v_f / \alpha_f$ is the Prandtl number, $\beta_T = 1/c\tau_T$ is the fluid particle interaction parameter for temperature, $Ec = cl^2 / \mathrm{A}(c_p)_f$ is the Eckert Number, and $\gamma = (c_p)_f / c_m$ is the ratio of the specific heat of the fluid to dust particles.

For engineering interests, the skin friction coefficient C_f and the local Nusselt number Nu_x are defined as;

$$C_f = \tau_w / \rho_f u_w^2, Nu_x = xq_w / k_f(T_w - T_\infty) \tag{19}$$

where the surface shear stress τ_w and the surface heat flux q_w are given by;

$$\tau_w = \mu_{nf}\left(\frac{\partial u}{\partial y}\right)_{y=0}, \; q_w = -k_{nf}\left(\frac{\partial T}{\partial y}\right)_{y=0} \tag{20}$$

Using non-dimensional variables, we obtain;

$$C_f \,\mathrm{Re}_x^{1/2} = \frac{1}{(1-\phi)^{2.5}} f''(0), \mathrm{Nu}_x \,\mathrm{Re}_x^{-1/2} = -\frac{k_{nf}}{k_f}\theta'(0) \tag{21}$$

where $\mathrm{Re}_x = u_w x / v_f$ is the local Reynolds number.

Numerical procedure

The system of nonlinear ordinary differential equations in Eqs. (8), (9) and Eqs. (16), (17), with the boundary conditions in Eq. (11) and Eq. (18), respectively, are solved numerically using a Runge-Kutta based shooting technique (Sandeep and Sulochana [30]). We considered $f = x_1, f' = x_2, f'' = x_3, F = x_4, F' = x_5, \theta = x_6, \theta' = x_7, \theta_p = x_8, \theta'_p = x_9$, Eqs. (8), (9) and Eqs. (16), (17) are transformed into systems of first order differential equations. Subject to the following initial conditions;

$$x_1(0) = S \;\; x_2(0) = \lambda, \; x_3(0) = s_1, x_4(0) = -S, \; x_5(0) = s_2, \; x_7(0) = s_3 ..etc. \tag{22}$$

We assumed the unspecified initial conditions in Eq. (22), and the transformed first order differential equations are integrated numerically as an initial valued problem at a given terminal point. We checked the accuracy of the assumed missing initial condition by comparing them with the calculated

value of the different variable at the terminal point. The calculations are carried out using the Matlab programme.

Results and discussion

The system of nonlinear ordinary differential equations in Eqs. (8), (9) and Eqs. (16), (17), with the boundary conditions in Eq. (11) and Eq. (18), respectively, are solved numerically using a Runge-Kutta based shooting technique. The results show the effects of non-dimensional governing parameters, namely magnetic field parameter (M), volume fraction of dust particles (ϕ_d), volume fraction of nanoparticles (ϕ), mass concentration of dust particles (α), fluid particle interaction parameter for velocity (β), fluid particle interaction parameters for temperature (β_T), and non-uniform heat source/sink parameters $(A^* \text{ and } B^*)$ on velocity and temperature profiles, for both fluid and dust phases and for stretching and shrinking cases, and are presented graphically. Also, skin friction coefficient and Nusselt number are discussed and presented in tabular form. For numerical results, we used $A^* = B^* = \alpha = \beta = 0.5$, $\phi_d = \phi = 0.1$, $\text{Pr} = 6.2$, $\beta_T = 0.2, Ec = 0.2, \gamma = 0.01$. These values were common for the entire study, except for the varied values in the respective figures. This study explores a detailed analysis of the momentum and heat transfer characteristics of TiO_3-water and Al_2O_3-water nanofluids embedded with dust particles. For the momentum and heat transfer behaviour, we highlighted the results in indexed figures. The thermophysical properties of the base fluid and the particles are depicted in **Table 1**.

Table 1 Thermophysical properties of base fluid and different nanoparticles.

	$\rho(Kg\,m^{-3})$	$c_p(J\,Kg^{-1}\,K^{-1})$	$k\,(Wm^{-1}\,K^{-1})$
Water (H_2O)	997.1	4179	0.613
Titanium oxide (TiO_2)	4250	686.2	8.9538
Aluminium oxide (Al_2O_3)	3970	765	40

Figures 2 - 5 depict the effect of magnetic field parameter (*M*) on velocity and temperature profiles of the fluid and dust phases for stretching and shrinking cases. From **Figures 2** and **3**, an increase in magnetic field parameter decreases the velocity profiles of both dusty nanofluids in the stretching case, but this is reversed in the shrinking case. Generally, increases in magnetic field generate an opposite force to the flow, called the Lorentz force. This force may slow down the velocity of the fluid in the stretching case, but it may act in the reverse manner in the shrinking case. This is the reason we notice an increase in velocity profiles by an increase in magnetic field in the shrinking case. Similar results are observed from **Figure 5** but, from **Figure 4**, it is interesting to note that increase in magnetic field parameter enhances the temperature profiles of the fluid phase in the stretching surface. We also observe a significant hike in temperature profiles of the Al_2O_3-water dusty nanofluid, compared with TiO_2-water dusty nanofluid.

Figures 6 - 9 illustrate the velocity and temperature profiles of fluid and dust phases over stretching/shrinking surfaces for various values of volume fractions of nanoparticles (ϕ). From **Figure 6** and **Figure 7**, it is observed that increasing the value of volume fraction of nanoparticles increases the velocity profiles of the fluid and dust phases in the stretching surface and decreases in the shrinking surface. From **Figure 6**, in the shrinking case, we notice an interesting result, where the influence of nano particle volume fraction is initially higher on Al_2O_3-water dusty nanofluid, but for higher values of ϕ, we

see that TiO_2-water dusty nanofluid is more affected by ϕ, compared with Al_2O_3-water dusty nanofluid. It is evident from **Figures 8** and **9** that increases in volume fraction of nanoparticles enhances the temperature profiles of both fluid and dust phases in the stretching case, but enhancement in ϕ decreases the temperature profiles in the shrinking case. This phenomenon can be explained by the fact that increases in ϕ cause improvement in thermal conductivity. This enhancement in thermal conductivity increases the thermal and velocity boundary layer thicknesses.

Figures 10 - 13 show the effect of volume fraction of dust particles (ϕ_d) on velocity and temperature profiles of the fluid and dust phases for stretching and shrinking cases. It is clear from **Figures 10 - 11** that the velocity profiles of fluid and dust phases decrease in the stretching sheet, and increase in the shrinking sheet, by the increase in the volume fraction of dust particles. This is due to the fact that, if the volume occupied by the dust particles is more, it then reduces the momentum boundary layer thickness in the stretching surface. It is evident from **Figures 12 - 13** that increase in the value of ϕ_d enhances the temperature profiles of the fluid phase and reduces the temperature profiles in the dust phase for the stretching case. In the shrinking case, we notice the opposite results. It is important to mention here that the increase/decrease in temperature profiles by the increase/decrease in volume fraction of dust particles is significantly less compared with the increase/decrease in the volume fraction of nanoparticles. Also, we notice an interesting result where enhancement in the value of volume fraction of nanoparticles uniformly improves temperature profiles in both dusty nanofluids, but increase in volume fraction of dust particles significantly improves the temperature profiles of Al_2O_3-water dusty nanofluid, compared with TiO_2-water dusty nanofluid. It is evident that the volume fraction of nanoparticles is more effective in enhancing the thermal boundary layer thickness compared with the volume fraction of dust particles. We clearly observe all these results from **Figures 8** and **12**.

The effect of mass concentration of dust particles (α) on the velocity and temperature profiles of the fluid and dust phases for stretching and shrinking cases is presented in **Figures 14 - 16**. It is observed from **Figures 14** and **15** that increase in mass concentration of dust particles decreases the velocity profiles of the fluid and particle phase for the stretching case. This is reversed in the shrinking case. Generally, increase in mass concentration of dust particles reduces heat transfer rate, which indirectly decreases the velocity boundary layer thickness in the stretching case. From **Figure 16**, we see that the enhanced value of α increases the temperature profiles of the fluid phase for the stretching case, and the opposite results are found in the shrinking case. We notice significant improvement in temperature profiles of Al_2O_3-water dusty nanofluid, compared with TiO_2-water dusty nanofluid, by increase in α. **Figures 17 - 19** display the effect of fluid particle interaction parameter for velocity (β) on the velocity and temperature profiles of the fluid and dust phases for stretching and shrinking cases. It is clear from these figures that increase in fluid particle interaction parameter for velocity depreciates the velocity and temperature profiles for fluid phase and improves the velocity and temperature profiles for dust phase in the stretching case. While coming to the shrinking case, we find increase in velocity profiles for fluid phase, and decrease in temperature and velocity profiles for fluid and particle phase. These may be due to an increase in fluid particle interaction, reducing the momentum and thermal boundary layer thickness for fluid phase and increasing for particle phase. Physical interaction of particles with the fluid dominates the velocity profiles of the base fluid. During this time, a force generates opposite to the flow field of the base fluid. This force slows down the velocity profiles until the particle phase reaches the fluid phase. The reason for increasing temperature profiles for dust phase is due to improved thermal conductivity by increase in interaction of the dust particles with nanoparticles.

The influence of fluid particle interaction parameter for temperature (β_T) on temperature profiles is shown in **Figure 20**. An increase in fluid particle interaction parameter for temperature enhances the temperature profiles in the stretching case, but this is reversed in the shrinking case. Physically, an increase in fluid particle interaction enhances the thermal conductivity of the flow. It is found that

increase in β_T helps to gradually enhance the temperature profiles of Al_2O_3-water dusty nanofluid, compared with TiO_2-water dusty nanofluid in the stretching case, but TiO_2-water dusty nanofluid shows better performance, with a hike in temperature, in the shrinking case.

Figures 21 and **22** reveal the effect of non-uniform heat source/sink parameters $(A^* \text{ and } B^*)$ on temperature profiles of the fluid phase for stretching and shrinking cases. Increases in $A^* \text{ and } B^*$ enhance the temperature profiles in the stretching case. Increase in A^* shows depreciation in temperature profiles in the shrinking case, but B^* helps to improve the temperature profiles in the shrinking case. It is evident that, for smaller values of $A^* \text{ and } B^*$, depreciation in temperature profiles is observed. This means the negative values of $A^* \text{ and } B^*$ act as heat observers, and positive values act as generators.

Table 2 Variation in $f''(0)$ and $-\theta'(0)$ for Al_2O_3-water dusty nanofluid at $\lambda = 1$.

M	ϕ	ϕ_d	α	β	β_T	A^* / B^*	$f''(0)$	$-\theta'(0)$
1							-2.100960	4.226665
2							-2.345788	4.270016
3							-2.563443	4.301333
	0.1						-2.100960	4.226665
	0.2						-1.913825	3.313793
	0.3						-1.680855	2.618675
		0.1					-2.100960	4.226665
		0.2					-2.149893	4.236108
		0.3					-2.211044	4.247338
			0.2				-1.997288	5.659212
			0.4				-2.032425	5.167767
			0.6				-2.066974	4.690494
				0.2			-2.003490	3.699356
				0.4			-2.040085	3.910121
				0.6			-2.072320	4.083036
					0.2		-2.100960	4.226665
					0.4		-2.100960	3.731753
					0.6		-2.100960	3.295211
						0.5	-2.100960	4.179087
						1.0	-2.100960	4.097954
						1.5	-2.100960	4.014451

Tables 2 and **3** shows the influence of non-dimensional governing parameters on skin friction coefficient $f''(0)$ and Nusselt number $-\theta'(0)$ for Al_2O_3-water and TiO_2-water dusty nanofluids. Increase in magnetic field parameter and volume fraction of dust particles depreciate the friction factor and improve the heat transfer rate for both dusty nanofluids. A rise in the value of volume fraction of nanoparticles increases the skin friction coefficient and reduces the Nusselt number. It is interesting to note that increase in fluid particle interaction parameter for velocity reduces the coefficient of skin friction and enhances the heat transfer rate. Increase in mass concentration of dust particles and fluid particle interaction parameter for temperature decreases the heat transfer rate, and change in the value of fluid particle interaction parameter for temperature does not have any influence on friction factor. The

non-uniform heat source/sink parameters do not have any influence on friction factor, but enhancing the values of A^* and B^* reduces the Nusselt number. **Table 4** shows the comparison of the present study with existing literature. We found an excellent agreement of the present results with the existing literature. This proves the validity of the present results, along with the accuracy of the present numerical technique.

Table 3 Variation in $f''(0)$ and $-\theta'(0)$ for TiO_2-water dusty nanofluid at $\lambda = 1$.

M	ϕ	ϕ_d	α	β	β_T	A^* / B^*	$f''(0)$	$-\theta'(0)$
1							-2.365389	4.388276
2							-2.121814	4.343329
3							-2.582141	4.421004
	0.1						-2.121814	4.343329
	0.2						-1.945742	3.483036
	0.3						-1.716094	2.808655
		0.1					-2.121814	4.343329
		0.2					-2.170489	4.353093
		0.3					-2.231335	4.364725
			0.2				-2.018657	5.822374
			0.4				-2.053614	5.315028
			0.6				-2.087991	4.822261
				0.2			-2.024797	3.802981
				0.4			-2.061200	4.018766
				0.6			-2.093287	4.195989
					0.2		-2.121814	4.343329
					0.4		-2.121814	3.830459
					0.6		-2.121814	3.378632
						0.5	-2.121814	4.294916
						1.0	-2.121814	4.212442
						1.5	-2.121814	4.127529

Table 4 Comparison of the results for wall temperature gradient $-\theta'(0)$ in the case of $\beta = \beta_T = Ec = \phi_p = \phi = A^* = B^* = 0$.

Pr	Gireesha *et al.* [19]	Present study
0.72	1.0886	1.0887
1	1.3333	1.3333
10	4.7968	4.7969

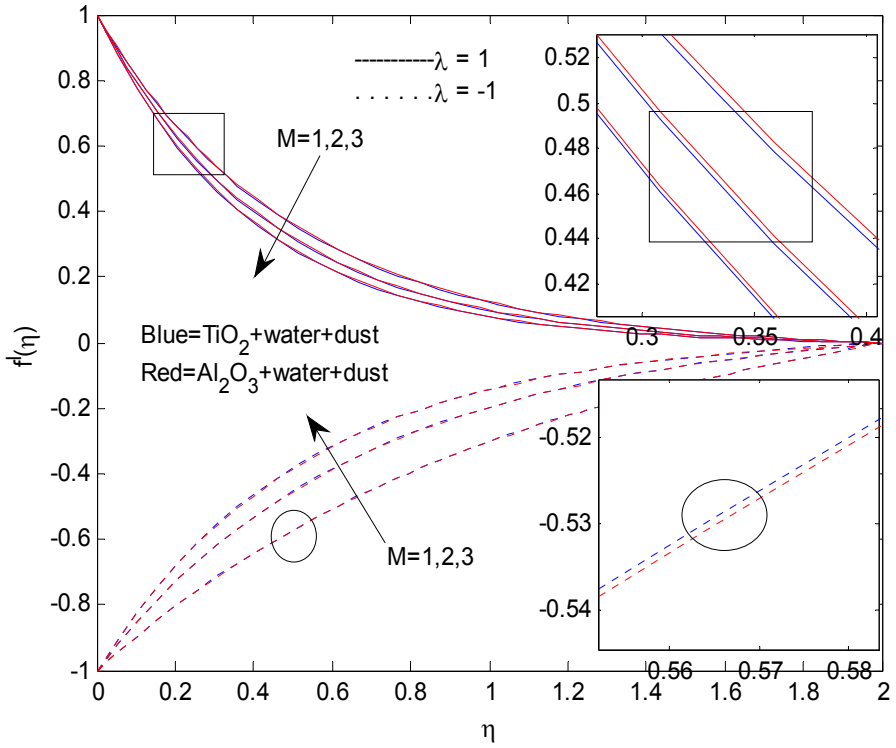

Figure 2 Velocity profiles of the fluid phase for various values of M .

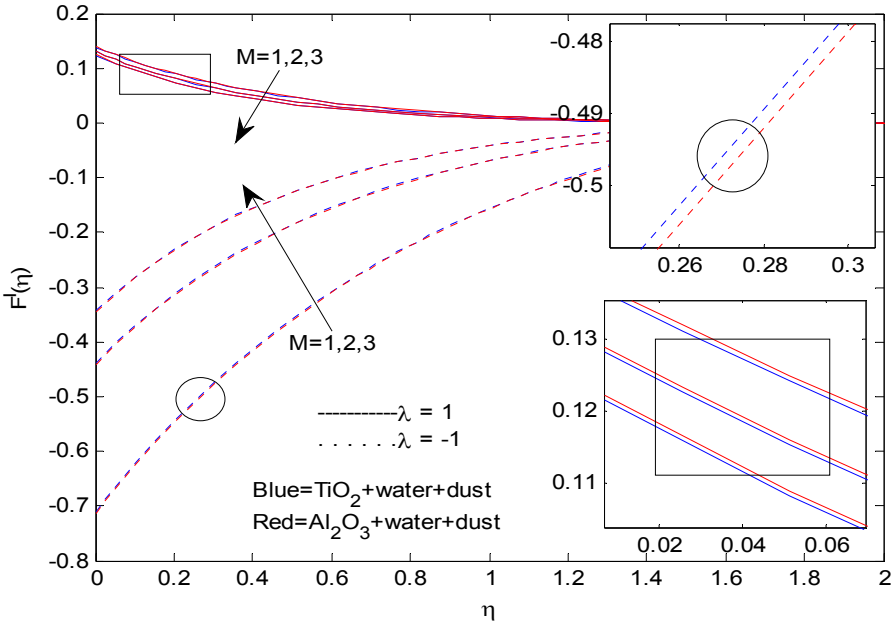

Figure 3 Velocity profiles of the dust phase for various values of M .

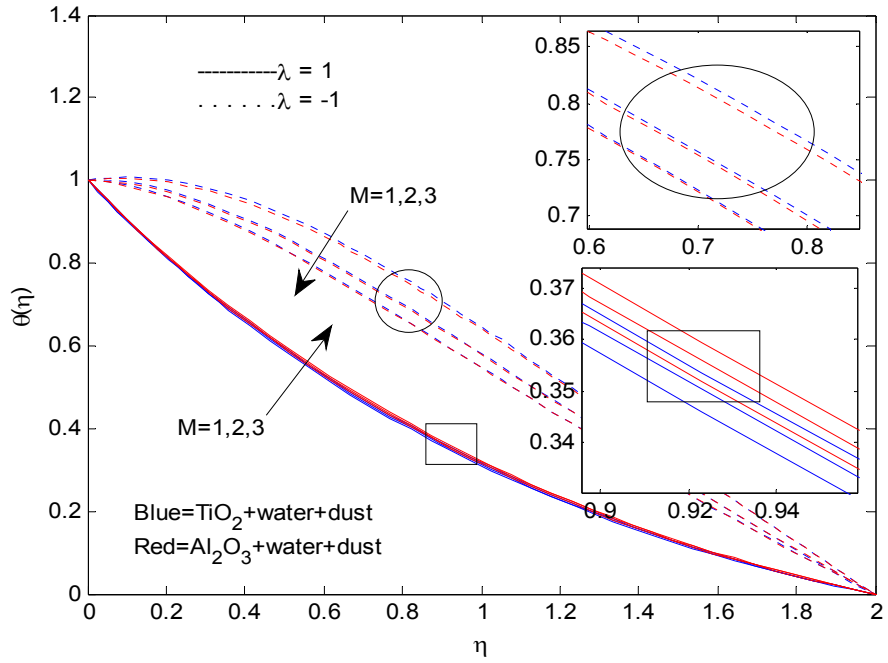

Figure 4 Temperature profiles of the fluid phase for various values of M .

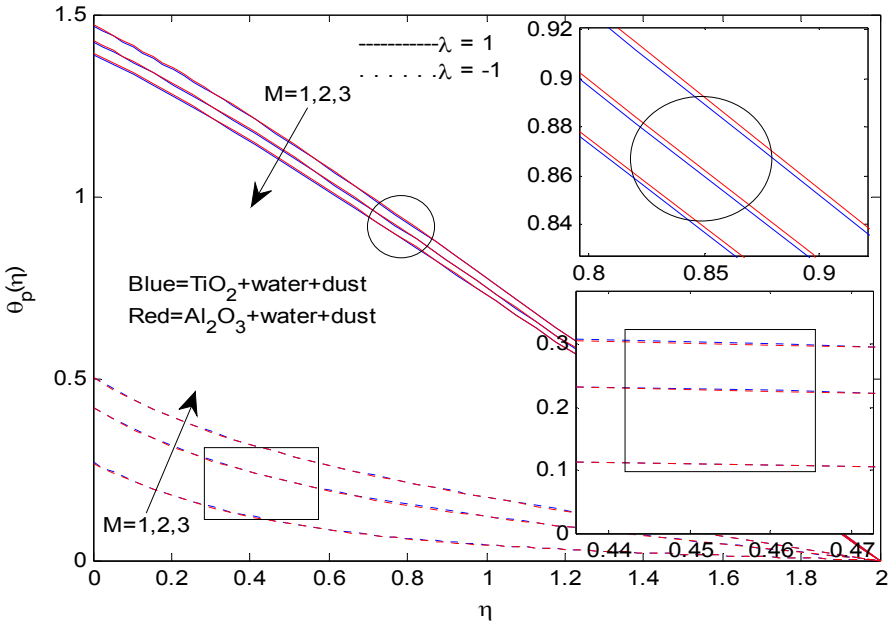

Figure 5 Temperature profiles of the dust phase for various values of M .

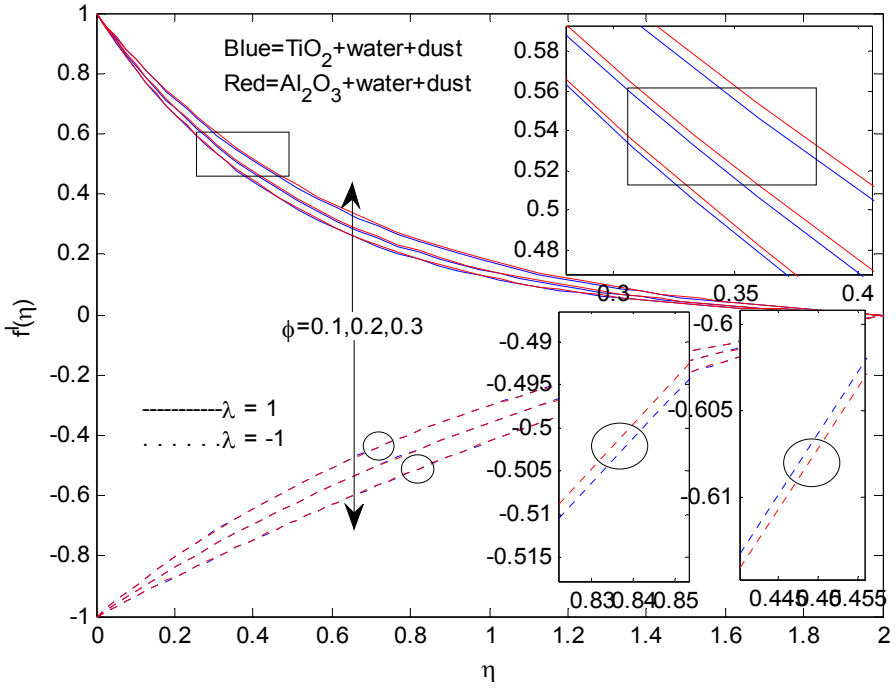

Figure 6 Velocity profiles of the fluid phase for various values of ϕ.

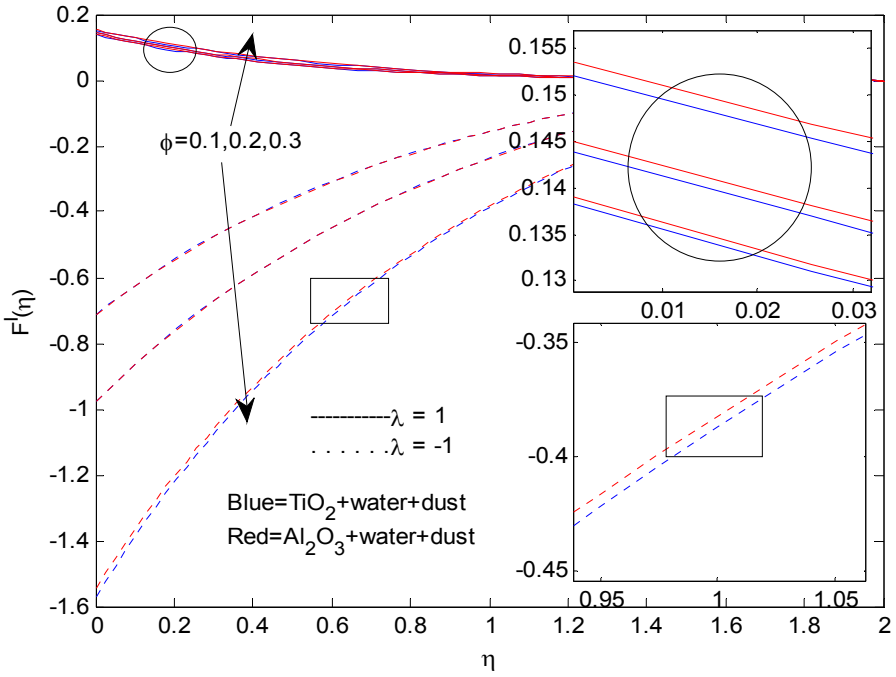

Figure 7 Velocity profiles of the dust phase for various values of ϕ.

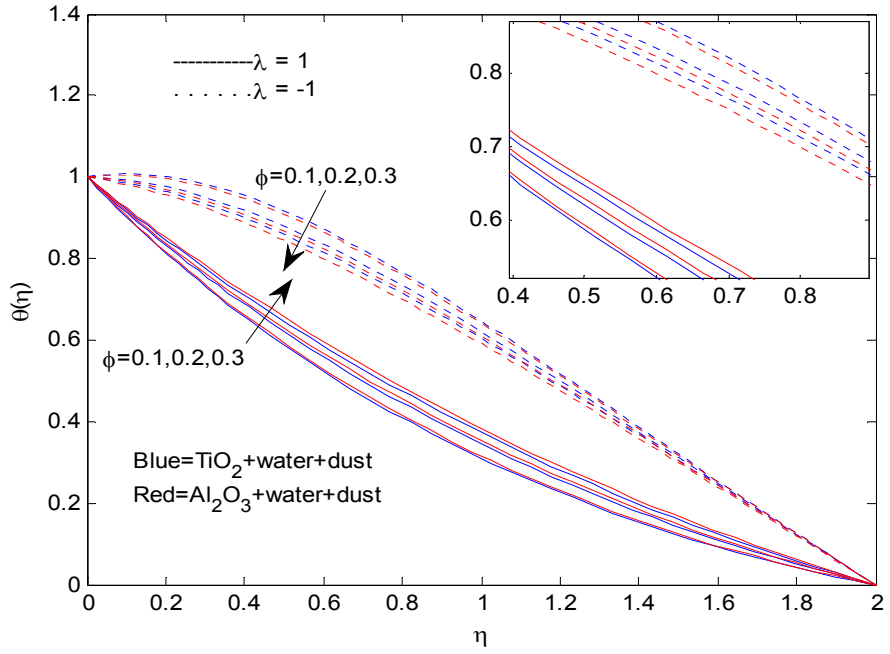

Figure 8 Temperature profiles of the fluid phase for various values of ϕ.

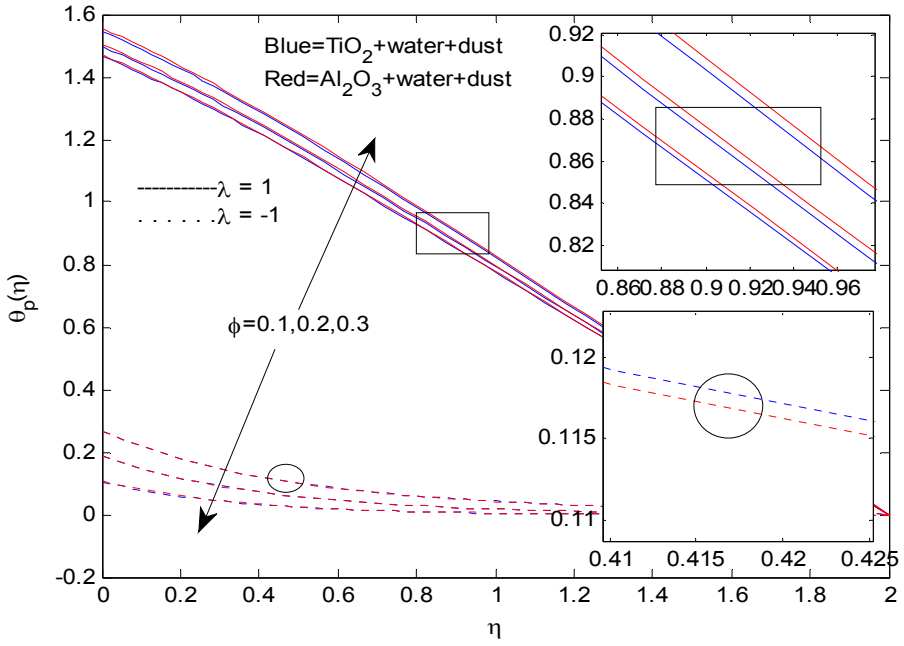

Figure 9 Temperature profiles of the dust phase for various values of ϕ.

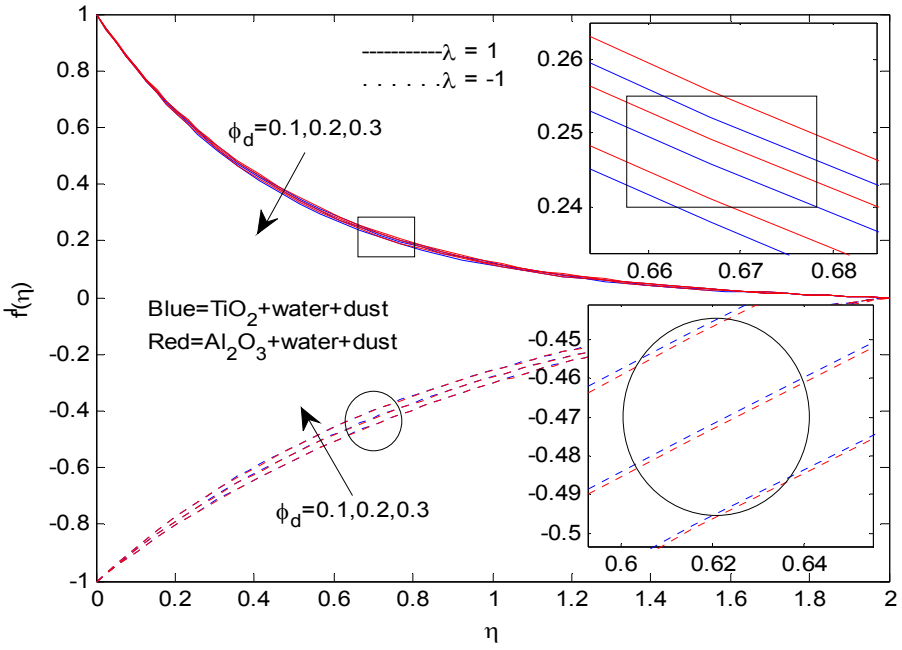

Figure 10 Velocity profiles of the fluid phase for various values of ϕ_d .

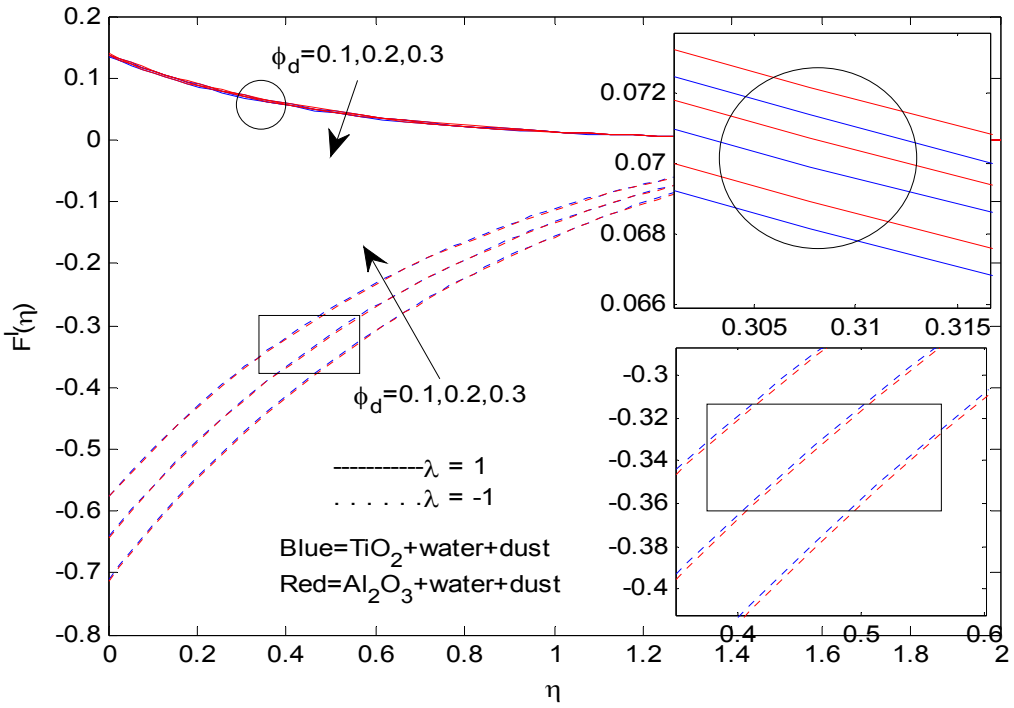

Figure 11 Velocity profiles of the dust phase for various values of ϕ_d .

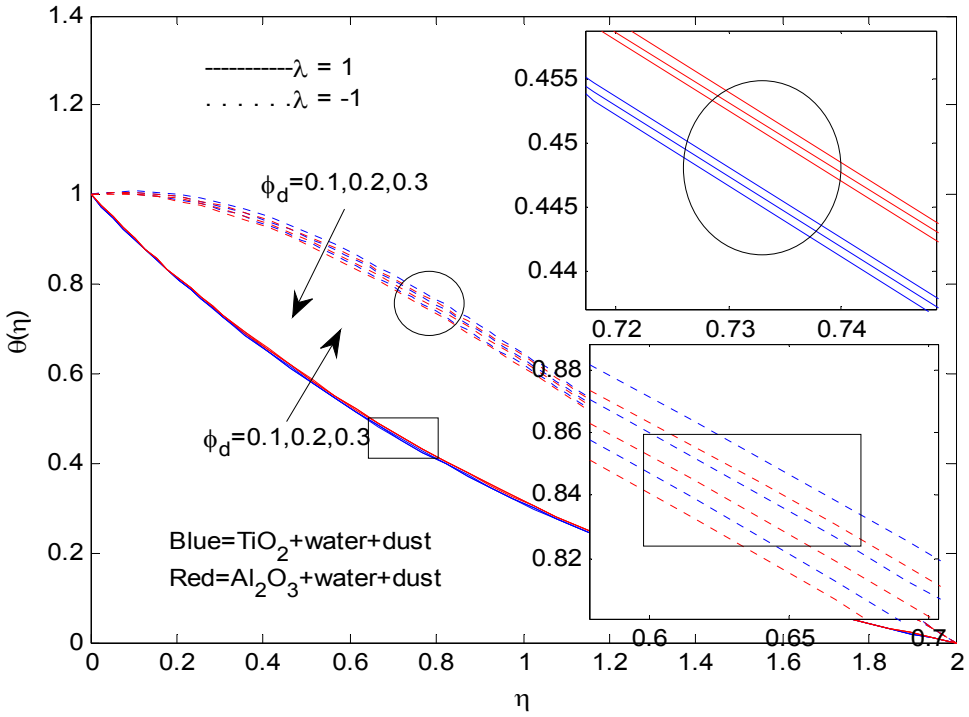

Figure 12 Temperature profiles of the fluid phase for various values of ϕ_d .

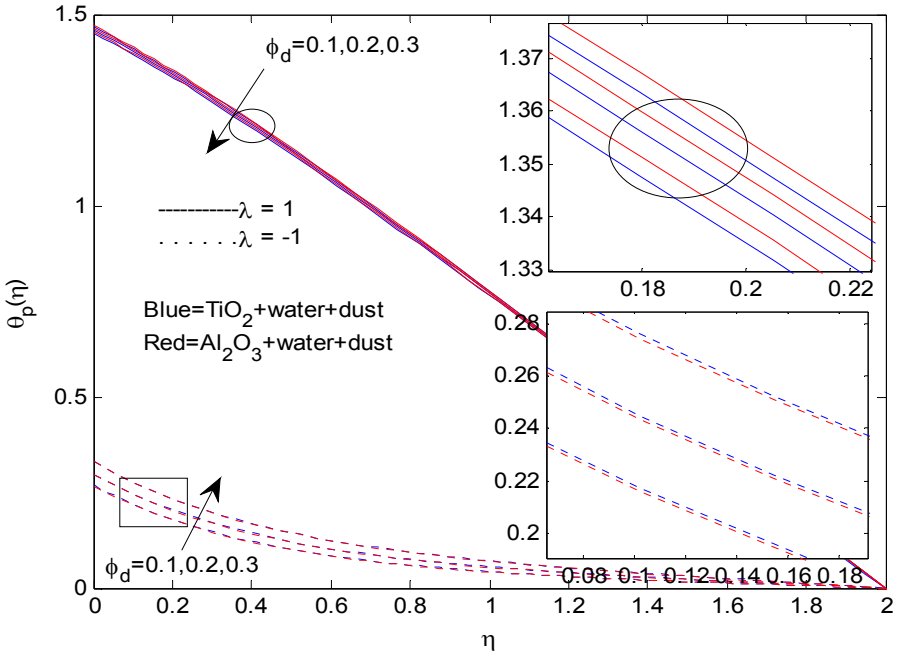

Figure 13 Temperature profiles of the dust phase for various values of ϕ_d .

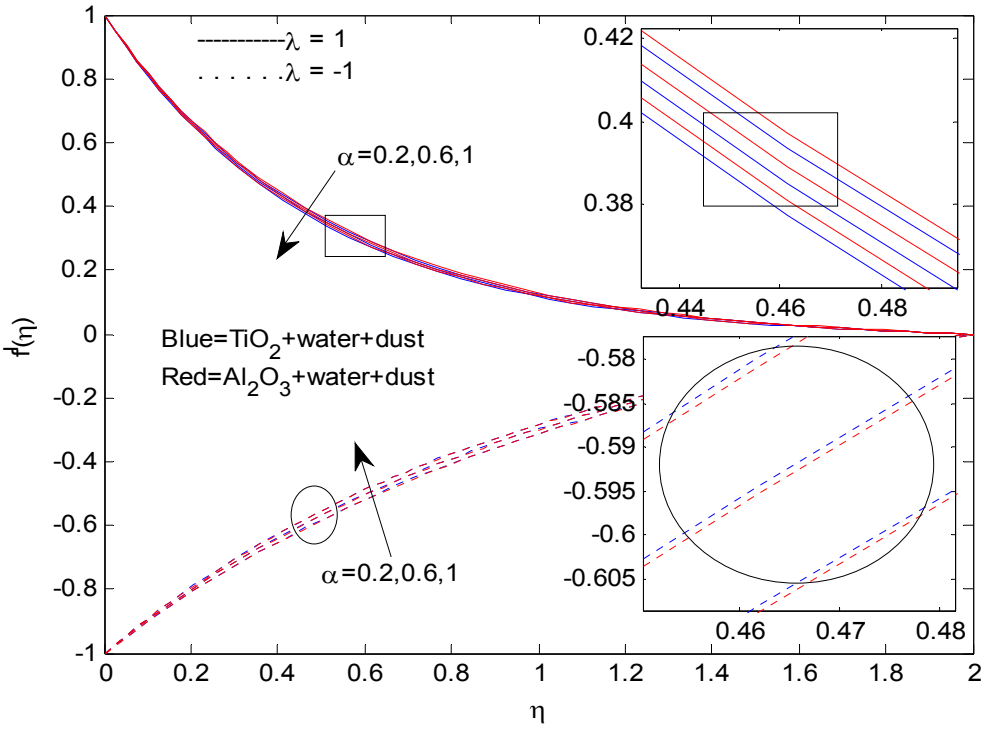

Figure 14 Velocity profiles of the fluid phase for various values of α .

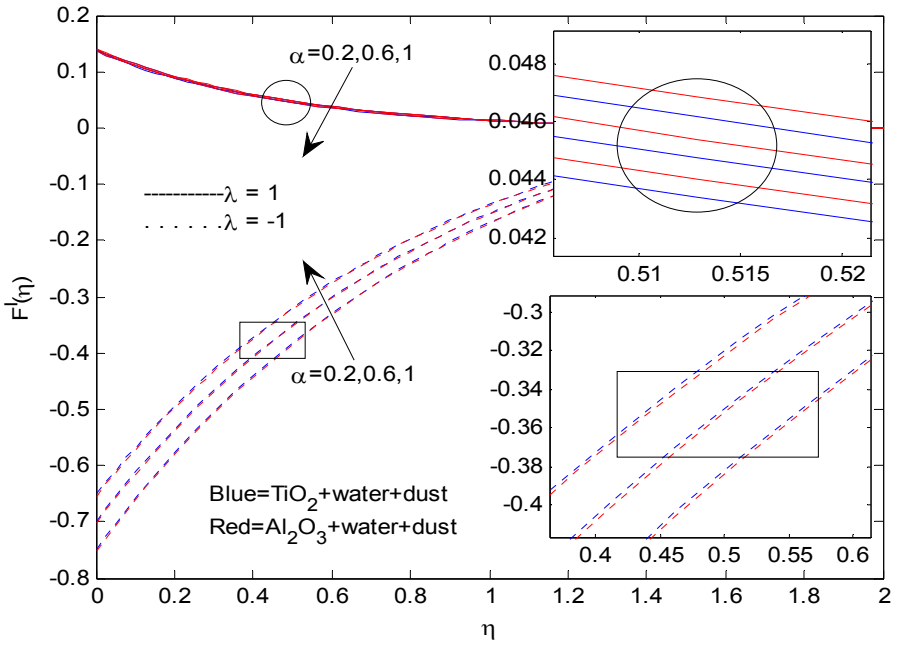

Figure 15 Velocity profiles of the dust phase for various values of α .

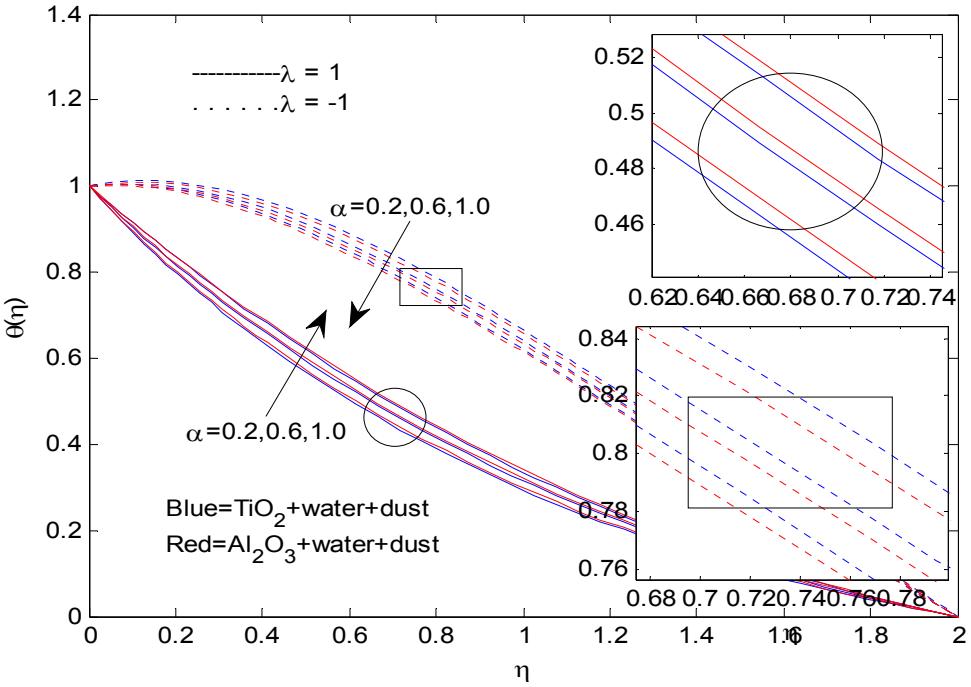

Figure 16 Temperature profiles of the fluid phase for various values of α .

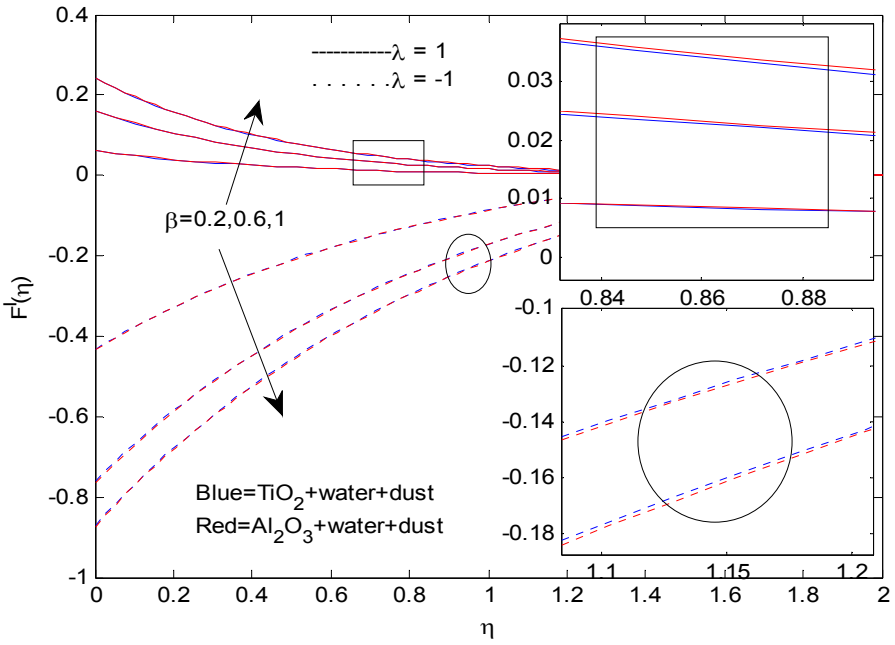

Figure 17 Velocity profiles of the dust phase for various values of β .

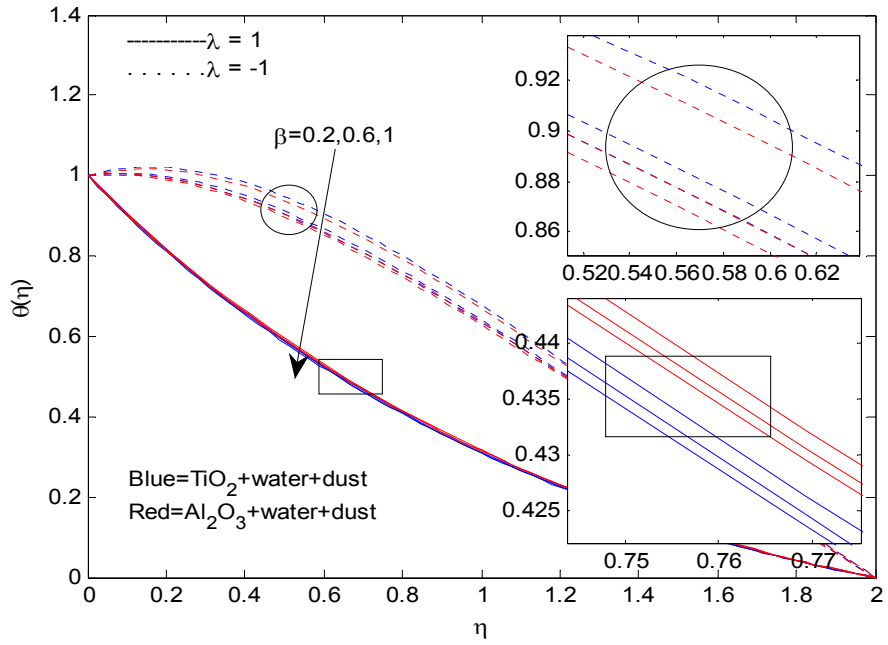

Figure 18 Temperature profiles of the fluid phase for various values of β .

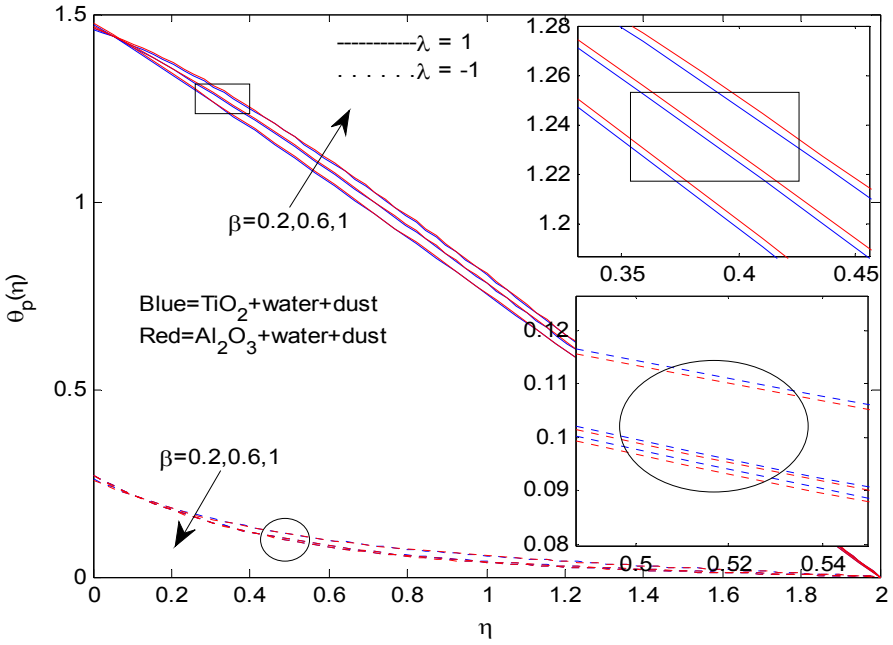

Figure 19 Temperature profiles of the dust phase for various values of β .

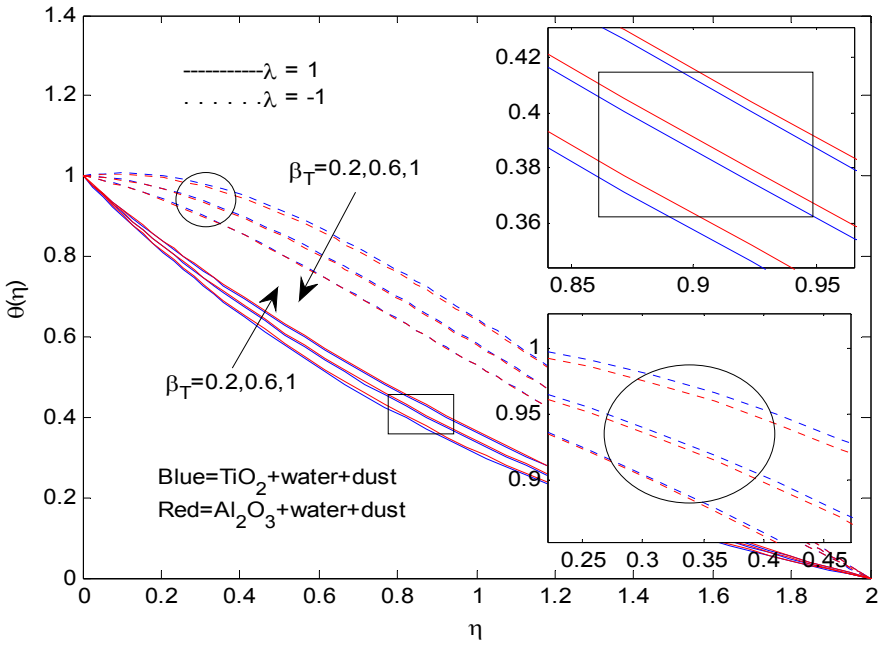

Figure 20 Temperature profiles of the fluid phase for various values of β_T .

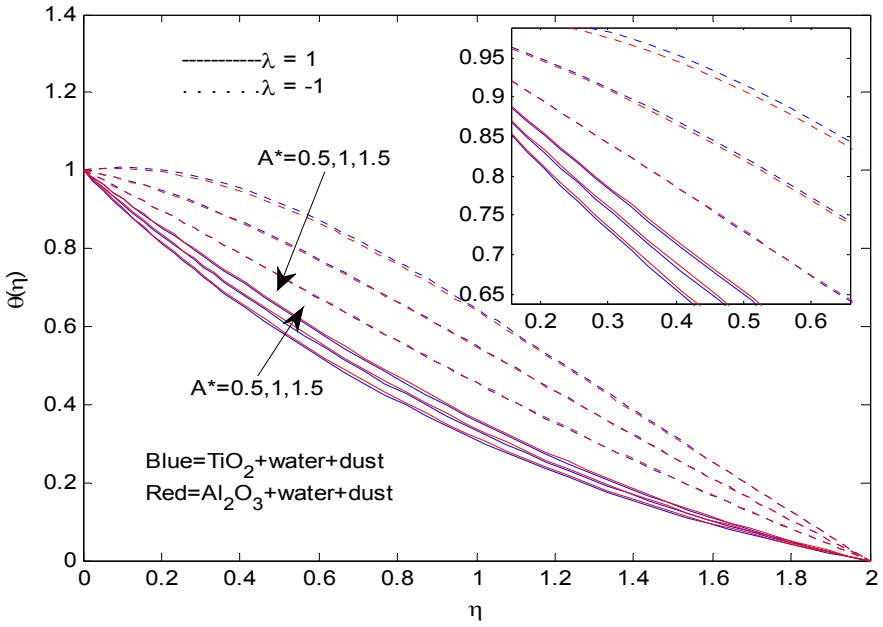

Figure 21 Temperature profiles of the fluid phase for various values of A^* .

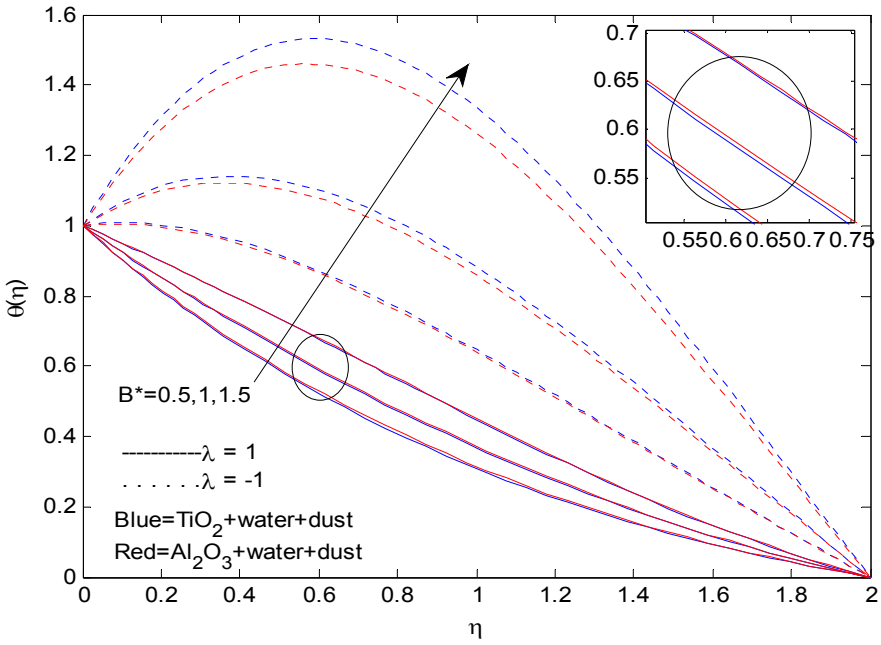

Figure 22 Temperature profiles of the fluid phase for various values of B^*.

Conclusions

In this study, we analyzed momentum and heat transfer characteristics of MHD flow of a dusty nanofluid over a permeable stretching/shrinking surface in the presence of a volume fraction of dust and nanoparticles with non-uniform heat source/sink. We considered TiO_2-water and Al_2O_3-water nanofluids immersed with dust particles. The effects of non-dimensional governing parameters on velocity and temperature profiles for both fluid and dust phases were discussed and presented through graphs. Also, skin friction coefficient and Nusselt number were discussed and presented for 2 dusty nanofluids separately in tabular form. The conclusions of the present study are as follows:

- Fluid particle interaction parameter for velocity has the capability to enhance the heat transfer rate of TiO_2-water and Al_2O_3-water dusty nanofluids for both stretching and shrinking surfaces.
- Increase in volume fraction of dust particles and volume fraction of nanoparticles improves the temperature profiles of both dusty nano fluids. This effect is high on Al_2O_3-water dusty nanofluid, compared with TiO_2-water dusty nanofluid in the stretching surface, and is reversed in the shrinking surface.
- Magnetic field parameter has the tendency to reduce the velocity boundary layer of the fluid phase. Increase in magnetic field parameter helps to enhance the heat transfer rate in the shrinking surface.
- Enhancement in mass concentration of dust particles decreases the friction factor and heat transfer rate in the stretching surface and improves the friction factor, along with Nusselt number, in the shrinking surface.
- A rise in the value of fluid particle interaction parameter for temperature does not have any influence on velocity profiles or skin friction coefficient, but it helps to enhance the heat transfer rate in the shrinking surface.
- Increases in volume fraction of nanoparticles help to uniformly enhance temperature profiles of both dusty nanofluids, but increases in volume fraction of dust particles show significant enhancement in the temperature profiles of Al_2O_3-water dusty nanofluid, compared with TiO_2-water dusty nanofluid, over the stretching surface.

• The increase/decrease in temperature/velocity profiles of the fluid or dust phases are less affected by enhancement in volume fraction of dust particles, compared with volume fraction of nanoparticles.

• The positive values of non-uniform heat source/sink parameters act like heat generators, and negative values act like heat observers.

• Al_2O_3-water dusty nanofluid dominated TiO_2-water dusty nanofluid in the stretching case, and TiO_2-water dusty nanofluid overtakes Al_2O_3-water dusty nanofluid in the shrinking case, in both velocity and temperature profiles.

Acknowledgements

The authors wish to express their sincere thanks to anonymous reviewers and editors in improving the manuscript. The First and Second authors acknowledge the UGC for their financial support under the UGC Dr. D.S. Kothari Fellowship Scheme (No.F.4-2/2006 (BSR)/MA/13-14/0026).

References

[1] PG Saffman. On the stability of laminar flow of a dusty gas. *J. Fluid Mech*. 1962; **13**, 120-8.
[2] FE Marble. Dynamics of dusty gases. *Annu. Rev. Fluid Mech*. 1970; **2**, 397-446.
[3] A Charkrabarti and AS Gupta. Hydro magnetic flow and heat transfer over a stretching sheet. *Quart. Appl. Math*. 1979; **37**, 73-8.
[4] SUS Choi. Enhanced thermal conductivity of nanofluids with nano particles. *In*: Proceedings of the 1995 ASME International Mechanical Engineering Congress and Exposition, San Francisco, USA, 1995, p. 99-105.
[5] AK Singh and NP Singh. MHD flow of a dusty viscoelastic liquid through a porous medium between two inclined parallel plates. *Proc. Natl Acad. Sci. India* 1996; **66**, 143-50.
[6] CH Chen. Laminar mixed convection adjacent to vertical, continuously stretching sheets. *Heat Mass Trans*. 1998; **33**, 471-6.
[7] DC Dalal, N Datta and SK Mukherjea. Unsteady natural convection of a dusty fluid in an infinite rectangular channel. *Int. J. Heat Mass Trans*. 1998; **41**, 547-62.
[8] HA Attia. Unsteady MHD couette flow and heat transfer of dusty fluid with variable physical properties. *Appl. Math Comput*. 2006; **177**, 308-18.
[9] J Buongiorno. Convective transport in nanofluids. *J. Heat Trans*. 2006; **128**, 240-50.
[10] SK Das, SU Choi, W Yu and T Pradeep. *Nanofluids: Science and Technology*. Willey, New Jersey, 2007.
[11] XQ Wang and AS Mujumdar. Heat transfer characteristics of nanofluids: A review. *Int. J. Therm. Sci*. 2007; **46**, 1-19.
[12] M Subhas Abel, E Sanjayanand and MM Nandeppanavar. Viscoelastic MHD flow and heat transfer over a stretching sheet with viscous and ohmic dissipations. *Commun. Nonlinear Sci. Numer. Simulat*. 2008; **13**, 1808-21.
[13] A Ishak, R Nazarand and I Pop. Heat Transfer over an unsteady stretching permeable surface with prescribed wall temperature. *Nonlinear Anal. Real World Appl*. 2009; **10**, 2909-13.
[14] KV Prasad, K Vajravelu and PS Datti. The effect of variable fluid properties on the hydromagnetic flow and heat transfer over a nonlinearly stretching sheet. *Int. J. Therm. Sci*. 2010; **49**, 603-10.
[15] I Saidu and MM Waziri. MHD effects on convective flow of dusty viscous fluid with volume fraction of dust particles. *J. Eng. Appl. Sci*. 2010; **5**, 86-91.
[16] OD Makinde and A Aziz. Boundary layer flow of a nanofluid past a stretching sheet with convective boundary condition. *Int. J. Therm. Sci*. 2011; **50**, 1326-32.
[17] MAA Hamad and I Pop. Unsteady MHD free convection flow past a vertical permeable flat plate in a rotating frame of reference with constant heat source in a nanofluid. *Heat Mass Trans*. 2011; **47**, 1517-24.

[18] MAA Hamad and M Ferdows. Similarity solution of boundary layer stagnation-point flow towards a heated porous stretching sheet saturated with nanofluid with heat absorption/generation and suction/blowing: A lie group analysis. *Commun. Nonlinear Sci. Numer. Simulat*. 2012; **17**, 132-40.
[19] BJ Gireesha, GS Roopa, HJ Lokesh and CS Bagewadi. MHD flow and heat transfer of a dusty fluid over a stretching sheet. *Int. J. Phys. Math. Sci.* 2012; **3**, 171-80.
[20] A Remeli, NM Arifin, F Ismail and I Pop. Marangoni-driven boundary layer flow in a nanofluid with suction/injection. *World Appl. Sci. J*. 2012; **17**, 21-6.
[21] K Zaimi, A Ishak and I Pop. Flow past a permeable stretching/shrinking sheet in a nanofluid using two phase model. *Plos One* 2014; **9**, e111743.
[22] MS Ferdows, M Chapal and AA Afify. Boundary layer flow and heat transfer of a nanofluid over a permeable unsteady stretching sheet with viscous dissipation. *J. Eng. Thermophys*. 2014; **23**, 216-28.
[23] A Malvandi, F Hedayati and DD Ganji. Slip effects on unsteady stagnation point flow of nanofluid over a stretching sheet. *Powder Tech*. 2014; **253**. 377-84.
[24] AM Rohni, S Ahmad and I Pop. Flow and heat transfer at a stagnation point over an exponentially shrinking vertical sheet with suction. *Int. J. Therm. Sci*. 2014; **75**, 164-70.
[25] SV Subhashini, R Sumathi and E Momoniat. Dual solutions of a mixed convection flow near the stagnation point region over an exponentially stretching/shrinking sheet in nanofluids. *Meccanica* 2014; **49**, 2467-78.
[26] MR Krishnamurthy, BC Prasannakumara, BJ Gireesha and RSR Gorla. Effect of viscous dissipation on hydromagnetic fluid flow and heat transfer of nanofluid over an exponentially stretching sheet with fluid-particle suspension. *Cogent Math*. 2015; **2**, 1050973.
[27] MR Krishnamurthy, BC Prasannakumara, BJ Gireesha and RSR Gorla. Effects of chemical reaction on MHD boundary layer flow and melting heat transfer of Williamson nanofluid in a porous medium. *Int. J. Eng. Sci. Tech.* 2016; **19**, 53-61.
[28] RSR Gorla and BJ Gireesha. Dual solutions for stagnation-point flow and convective heat transfer of a Williamson nanofluid past a stretching/shrinking sheet. *Heat Mass Trans*. 2016; **52**, 1153-62.
[29] N Sandeep and C Sulochana. MHD flow of a dusty nanofluid over a stretching surface with volume fraction of dust particles. *Ain Shams Eng. J*. 2016; **7**, 709-16.
[30] N Sandeep and C Sulochana. Dual solutions for unsteady mixed convection flow of MHD micropolar fluid over a stretching/shrinking sheet with non-uniform heat source/sink. *Int. J. Eng. Sci. Tech.* 2015; **18**, 738-45.
[31] P Mohan Krishna, N Sandeep and V Sugunamma. Effects of radiation and chemical reaction on MHD convective flow over a permeable stretching surface with suction and heat generation. *Walailak J. Sci. & Tech*. 2015; **12**, 831-47.
[32] Z Abbas, A Majeed and T Javed. Thermal radiation effects on MHD flow over a stretching cylinder in a porous medium. *Heat Trans. Res*. 2013; **44**, 703-18.
[33] T Javid and I Mustafa. Effects of unsteady expansion/contraction of Wang's cylinder problem with suction near a stagnation point. *Asia Pac. J. Chem. Eng*. 2015; **10**, 184-92.
[34] I Mustafa, T Javed and A Majeed. Magnetohydrodynamic (MHD) mixed convection stagnation point flow of a nanofluid over a vertical plate with viscous dissipation. *Can. J. Phys*. 2015; **93**, 1-10.